

---

# Integrating Flexible Normalization into Mid-Level Representations of Deep Convolutional Neural Networks

---

**Luis Gonzalo Sanchez Giraldo**  
 Department of Computer Science  
 University of Miami  
 Coral Gables, FL 33146  
 lgsanchez@cs.miami.edu

**Odelia Schwartz**  
 Department of Computer Science  
 University of Miami  
 Coral Gables, FL 33146  
 odelia@cs.miami.edu

## Abstract

Deep convolutional neural networks (CNNs) are becoming increasingly popular models to predict neural responses in visual cortex. However, contextual effects, which are prevalent in neural processing and in perception, are not explicitly handled by current CNNs, including those used for neural prediction. In primary visual cortex, neural responses are modulated by stimuli spatially surrounding the classical receptive field in rich ways. These effects have been modeled with divisive normalization approaches, including flexible models where spatial normalization is recruited only to the degree responses from center and surround locations are deemed statistically dependent. We propose a flexible normalization model applied to mid-level representations of deep CNNs as a tractable way to study contextual normalization mechanisms in mid-level visual areas. This approach captures non-trivial spatial dependencies among mid-level features in CNNs, such as those present in textures and other visual stimuli that arise from tiling high order features, geometrically. We expect that the proposed approach can make predictions about when spatial normalization might be recruited in mid-level cortical areas. We also expect this approach to be useful as part of the CNN toolkit, therefore going beyond more restrictive fixed forms of normalization.

## 1 Introduction

It has long been argued that an important step in understanding the information processing mechanisms in the brain is to understand the nature of the input stimuli [2, 5]. Visual processing of natural images is a paradigmatic example that has been studied extensively [38, 46, 30, 16, 21]. Structure in images can be captured in the form of statistical dependencies among the responses of filters acting on the image at different scales, orientations, and spatial locations [6, 29, 21]. These regularities often manifest in a nonlinear fashion [37, 43, 45, 17]. Therefore, it is natural to think that neural processing systems employ nonlinear operations to exploit dependencies appropriately.

Both perception and neural responses are influenced by the spatial context, i.e., by stimuli that spatially surround a given point in space. Spatial contextual influences beyond the classical receptive field have been extensively documented for neurons in primary visual cortex [26, 34, 9, 10]. Models that are based on nonlinear statistical regularities across space in images have been able to capture some of these effects [32, 36, 40, 24, 47].

Here, we focus on divisive normalization, a nonlinear computation that has been regarded as a canonical computation in the brain [20, 8, 7]. From a coding perspective, divisive normalization acts as a transformation that reduces nonlinear dependencies among filter activation patterns in natural

stimuli [36]. Different forms of divisive normalization have been considered in modeling contextual interactions among cortical neurons. In its basic form, the divisive normalization operation is applied uniformly across the entire visual field. However, spatial context effects in primary visual cortex are better explained by a weighted normalization signal [9, 10, 36]. Recently, more sophisticated models that recruit normalization in a nonuniform fashion [13] have shown better generalization at predicting responses of V1 neurons to natural images [14]. The rationale behind this form of *flexible normalization* (and related predictive coding models of [40, 28]) is that contextual redundancies vary with stimulus. In the flexible normalization model, divisive normalization is therefore only recruited at points where the pool of responses (context) to an image are deemed statistically dependent. This relates to highlighting salient information by segmentation in regions of the image in which the spatial homogeneity breaks down [27].

As basic computational modules, it would be expected that non-linearities take place at different stages of the cortical processing hierarchy. However, studying these operations beyond the primary level, for instance understanding when normalization is recruited in natural images, has been rather difficult and only recently addressed in neurophysiology experiments [48]. In comparison to primary visual cortex, where different features such as orientation, spatial frequency and scale have a fairly well understood role in characterizing visual stimuli, the optimal stimulus space for mid-cortical levels is less well understood [31].

In this work, we propose the use of deep CNNs to study how flexible normalization, might work at intermediate level representations. CNNs have shown intriguing similarities to visual cortex [44]. In addition, CNNs have interestingly incorporated simple forms of normalization [23, 25, 33]. They can provide a tractable way to model representations that might be employed by mid-levels of the visual processing hierarchy. Here, we integrate flexible normalization into the AlexNet CNN architecture [25], although the approach can be applied to other CNN architectures. For mid-level representations, we show that incorporating flexible normalization can capture non-trivial spatial dependencies among features such as those present in textures, and more generally, geometric arrangements of features tiling the space. Our focus here is on developing the framework for the CNN and demonstrating the learned statistics and spatial arrangements that result for middle layers of the CNN. We expect the proposed approach can make predictions about when spatial normalization might be recruited in mid-level areas, and therefore will be useful for interplay with future neuroscience experiments as well as become a standard component in the CNN toolkit.

## 2 Normalization in deep neural nets

Recently, new forms of normalization have been introduced to the deep neural networks tool set [22, 3]. The motivation for these computations is different from the divisive normalization models in neuroscience, which are based on observations of neural responses. Batch normalization [22] is a popular technique aimed at removing the covariate shift over time (i.e., in batches) in each hidden layer unit, with the goal of accelerating training by maintaining global statistics of the layer activations. Layer normalization [3] on the other hand, employs averages across units in a given layer (and space in the case of convolutional networks) at every time step, introducing invariances in the network that benefit the speed of learning. Batch and layer normalization provide better conditioning of the signals and gradients that flow through the network, forward and backwards, and have been studied from these perspective.

Simple forms of divisive normalization that draw inspiration from neuroscience, such as those described in [23, 25], have been used to improve the accuracy of deep neural network architectures for object recognition. However, the empirical evaluation of deeper architectures in [39] reached a different conclusion showing that the inclusion of local response normalization (LRN) did not offer any significant gains in accuracy. One possible yet untested hypothesis for this case is that the increased depth may be able to account for some of the nonlinear behavior associated with LRN. Nevertheless, it is important to note that these empirical conclusions have only considered simple and fairly restrictive forms of normalization and measured their relevance solely in terms of classification accuracy<sup>1</sup>.

Recent work that attempts at unifying the different forms of normalization discussed above has started to reconsider the importance of normalization for object recognition, in the context of su-

---

<sup>1</sup>Robustness to adversarial examples seems as a potential way to evaluate the role of normalization.

pervised deep networks [33]. Divisive normalization approaches arising from a generative model perspective have also been recently introduced [4]. Other work on supervised networks inspired by primary visual cortex circuitry has proposed normalization as a way to learn discriminant saliency map between a target and its null class [18, 19]. Although these works extend beyond the simple normalization forms discussed in previous paragraphs, they are still limited to fixed normalization pools and to early stages of processing. None of these approaches have thus far considered the role of spatial dependencies and normalization in middle layers of CNNs to address questions in neuroscience.

Our work extends the class of flexible normalization models considered in [13, 14] which stem from a normative perspective where the division operation relates to (the inverse of) a generative model of natural stimuli. In previous work, flexible normalization models were learned for an oriented filter bank akin to primary visual cortical filters. We develop a flexible normalization model that can be applied to convolution filters in deep CNNs. Our objective in this paper is to develop the methodology and to study the statistical properties and the structure of the dependencies that emerge in middle layers (specifically, we focus on the second convolutional layer of a AlexNet). We expect our model to be useful in providing insights and plausible hypotheses about when normalization is recruited in visual cortical areas beyond Primary Visual Cortex.

## 2.1 Statistical model for divisive normalization

A characteristic of natural stimuli is that the coefficients obtained by localized linear decompositions such as wavelets or independent component analysis are highly non-Gaussian, generally depicting the presence of heavy tailed distributions [15]. In addition, these coefficients, even if linearly uncorrelated, still expose a form of dependency where the standard deviation of one coefficient can be predicted by the magnitudes of spatially related coefficients [37]. In this sense, models that extend beyond linearity are needed to deal with nonlinear dependencies that arise in natural stimuli.

A conceptually simple yet powerful generative model that can capture this form of coupling is known as the Gaussian Scale Mixture [1, 41, 42]. In this class of models, the multiplicative coordination between filter activations is captured by incorporating a common mixer variable. This is achieved by a statistical model that includes local Gaussian variables that are multiplied by a common mixer. After forming the generative model, one can reduce the dependencies and estimate the local Gaussian variables, via inversion (divisive normalization). The Gaussian variables may themselves be linearly correlated which amounts to a weighted normalization.

Formally, a vector  $X$  containing a set of  $m$  coupled activations is obtained by multiplying an independent positive scalar random variable  $V$  (which we denote the mixer variable) with an  $m$ -dimensional Gaussian random vector  $G$  with zero mean and covariance  $\Lambda$ , that is,  $X = VG$ . The random variable  $X|V = v$  is a zero mean Gaussian random variable with covariance  $\Lambda v^2$ , and  $X$  is distributed with pdf:

$$p_X(\mathbf{x}) = \int_0^\infty \frac{v^{-m}}{(2\pi)^{m/2} |\Lambda|^{1/2}} \exp\left(-\frac{\mathbf{x}^T \Lambda^{-1} \mathbf{x}}{2v^2}\right) p_V(v) dv. \quad (1)$$

For analytical tractability, we consider the case where the mixer  $V$  is a Rayleigh distributed random variable with pdf,  $p_V(v) = \frac{v}{h^2} \exp\left(-\frac{v^2}{2h^2}\right)$ , for  $v \in [0, \infty)$ , and scale parameter  $h$ . Integrating over  $v$  yields the following pdf:

$$p_X(\mathbf{x}) = \frac{1}{(2\pi)^{m/2} |\Lambda|^{1/2} h^m} a^{1-m/2} K_{m/2-1}(a), \quad (2)$$

where  $K_\lambda(\cdot)$  is the modified Bessel function of the second kind, and

$$a^2 = \frac{\mathbf{x}^T \Lambda^{-1} \mathbf{x}}{h^2}. \quad (3)$$

To ease notation, we can let  $\Lambda$  absorb the scale  $h$ . Reversing the above model to make inferences about  $G$  given  $X$  results in an operation similar to divisive normalization. Given an instance  $\mathbf{x}$  of  $X$ , we can compute the conditional expectation of the  $i$ th element of  $G$  as follows:

$$\mathbb{E}[g_i|\mathbf{x}] = \frac{x_i}{\sqrt{a}} \frac{K_{\frac{m-1}{2}}(a)}{K_{\frac{m}{2}-1}(a)}. \quad (4)$$

The divisive normalization is weighted, due to the term  $a$ , which incorporates the inverse of the covariance matrix in the computations of the normalization factor.

### 3 Flexible contextual normalization

The Gaussian Scale Mixture model described thus far assumes a single mixer variable capturing the coordination between filter activations (e.g., for receptive fields that lie in nearby spatial locations). The normalization operation produced by performing inference on the GSM model is replicated across the entire image intrinsically assumes the statistics to be homogeneous across space. However, the statistical dependency between filter activations may vary depending on the particular visual image and set of filters, such as if the filters cover a single visual object or feature, or are spaced across the border of objects in a given image [35].

A more sophisticated model [13], uses a two-component mixture of GSMs,

$$p_X(\mathbf{x}) = \Pi_{cs} p_X(\mathbf{x}|\Lambda_{cs}) + (1 - \Pi_{cs}) p_{X_c}(\mathbf{x}_c|\Lambda_c) p_{X_s}(\mathbf{x}_s|\Lambda_s), \quad (5)$$

where  $\mathbf{x}_c$  and  $\mathbf{x}_s$  denote the set of responses from units with receptive fields in center and surround locations, and  $\Lambda_{cs}$ ,  $\Lambda_c$ , and  $\Lambda_s$  are the parameters that capture covariant structure on the neural responses. In this model, normalization is only recruited to the degree center and surround responses are deemed as statistically dependent. The first term of (25),  $p_X(\mathbf{x}|\Lambda_{cs})$ , corresponds to center-surround dependent units, and the product  $p_{X_c}(\mathbf{x}_c|\Lambda_c) p_{X_s}(\mathbf{x}_s|\Lambda_s)$  in the second term represents the statistical independence between the center group and the surround group.

Different from [12], our model imposes statistical independence among surround responses in the center-surround independent component of the mixture by making

$$p_{X_s}(\mathbf{x}_s|\Lambda_s) = \prod_{\ell \in S} p_{(X_s)_\ell}((\mathbf{x}_s)_\ell | (\Lambda_s)_\ell). \quad (6)$$

Thus, when center units are independent from surround units, the surround units do not share the same mixer. A graphical model of the modified flexible normalization is depicted in Figure 1a. Since the model assumes decoupled responses of the surround units in the case of independence, there is no need to impose the symmetry constraints originally used in [12] for learning the parameters of the model. It is important to bear in mind that for mid-level representations there is no clear intuition or explicit knowledge about nature of the symmetries that may arise across space.

#### 3.1 Inference

Another key difference between our model and [35] is the inference. We assume the linear couplings among the Gaussian variables in the center-surround dependent component and among the Gaussian variables in the center-surround independent component are the result of applying two different linear transformations to the same underlying Gaussian variable  $\hat{G}$ . The  $\mathbb{E}[\hat{G}_i|\mathbf{x}]$  is obtained by a two-stage process. First, posterior probabilities of  $\mathbf{x}$  being center-surround dependent are obtained using Bayes rule,  $p(\xi_1|\mathbf{x}) = \frac{p(\mathbf{x}|\xi_1)\Pi_{cs}}{p(\mathbf{x})}$ . Then, conditional expectations  $\mathbb{E}[G_i|\mathbf{x}, \Lambda_{cs}]$  and  $\mathbb{E}[G_i|\mathbf{x}_c, \Lambda_c]$  are linearly mapped to a common space. Namely, we apply a linear transformation  $\mathbf{Q}^T$  to the center-surround independent component  $\mathbf{cs}_\perp$ , such that:

$$\mathbf{Q}^T \Lambda_{cs_\perp} \mathbf{Q} = \mathbf{Q}^T \left[ \begin{array}{c|c} \Lambda_c & \mathbf{0} \\ \hline \mathbf{0} & \Lambda_s \end{array} \right] \mathbf{Q} = \Lambda_{cs}, \quad (7)$$

Inference in our flexible normalization model is given by:

$$\mathbb{E}[\hat{G}_i|\mathbf{c}] = p(\xi_1|\mathbf{x}) \mathbb{E}[G|\mathbf{x}, \Lambda_{cs}] + (1 - p(\xi_1|\mathbf{x})) (\mathbf{Q}^T)_{i,:} \mathbb{E}[G|\mathbf{x}, \Lambda_c, \Lambda_s], \quad (8)$$

where  $(\mathbf{Q}^T)_{i,:}$  denotes the  $i$ th row of  $\mathbf{Q}^T$ . This inference can be followed by whitening of the components of  $\hat{G}$ . However, here, the relevant operation is the transformation that takes one covariance and makes it equal to the other covariance (7).

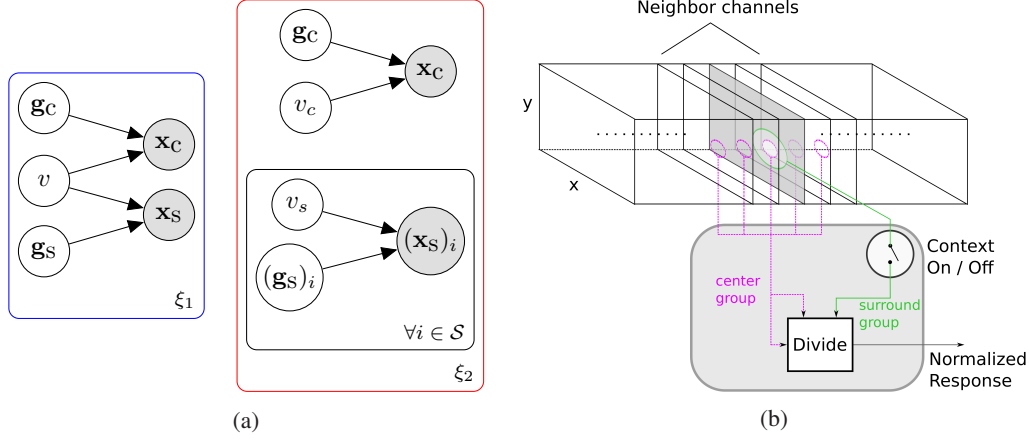


Figure 1: (a) Flexible normalization model, based on a mixture of Gaussian Scale Mixtures. (left) Center-Surround dependent; (right) Center-Surround Independent. The model is similar to [12, 14], except that when center units are independent from surround units, we further impose independence of the surround unit activations. This removes the need impose any symmetry constraints in learning the model parameters, which is critical for this approach to work in higher CNN layers beyond V1-like oriented filters. (b) Schematic of flexible normalization on map computed by a convolutional layer of a deep CNN. To compute the normalized response of a filter  $k$  at location  $(x, y)$ , the model uses responses from adjacent filters (channels) in the arrangement (akin to cross-orientation suppression in primary visual cortex) as the center group, and a set of responses from the same filter  $k$  at relative displacements from the  $(x, y)$  position to form the surround group (spatial context).

### 3.2 Convolutional layers and flexible normalization

In their most basic form, convolutional neural networks are a particular instance of feedforward networks with restrict set of the linear transformations by imposing local connectivity and weight sharing constraints. Convolutional layers of deep CNNs are arrangements of filters that process the input over the spatial dimensions. On 2-dimensional images, each of the CNN filters linearly transforms a collection of 2-dimensional arrays called input channels. For instance, RGB images are 2-dimensional images with 3 channels. The output produced by each filter is a 2-dimensional array of responses called a map. Therefore, each convolutional layer produces as many output maps as filters. Let  $I_{in}(x, y, \ell)$  be the collection of 2-d input arrays, where  $x$  and  $y$  denote the spatial indexes and  $\ell \in \mathcal{X}_{in}$  the input channel index<sup>2</sup>. A convolutional layer is a collection of 3-dimensional arrays  $\{W_k(x, y, \ell)\}_{k \in \mathcal{C}_{out}}$ . The operation of convolution, which yields a map, is defined as:

$$I_{out}(x, y, k) = \sum_{\ell} \sum_{x', y'} I_{in}(x + x', y + y', \ell) W_k(x', y', \ell) \quad (9)$$

In addition to convolutions and point-wise nonlinearities, CNNs can include other nonlinear operations such as pooling and normalization whose outputs depend on the activities of groups of neurons. Here, we cascade the flexible normalization model with the a convolution layer. Flexible normalization of the outputs of a convolutional layer is carried out at each spatial position and output channel of  $I_{out}$ . For channel  $k$  and spatial position  $(x, y)$ , the normalization pool consists of two groups: (i) a group of activations at the same  $(x, y)$  position from spatially overlapping filters from channels neighbor to  $k$ , called the center group; (ii) a set of spatially shifted neighboring channels called the surround group and denoted by  $\mathcal{N}_k$ . The surround group contains activations from channel  $k$  at spatial neighboring points to  $(x, y)$  denoted by  $\mathcal{N}_{(x, y)}$ . Figure 1b depicts this arrangement of maps produced by the filters in a convolutional layer as a 3-dimensional array. For each map  $k$ , we compute the normalized response at each  $(x, y)$  location using the flexible normalization model introduced above.

<sup>2</sup>It should be clear from the context where  $x$  refers to spatial location and not to a realization of  $X$

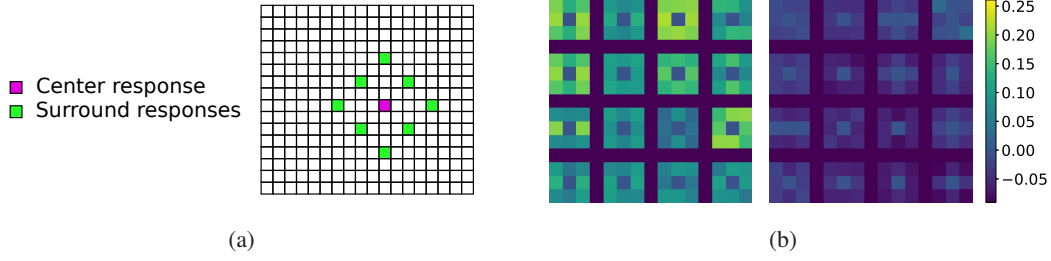


Figure 2: (a) Spatial distribution of center and surround activations in the normalization pool. (b) Correlation of energies between center and surround responses of Conv2 units from AlexNet before (left) and after (right) normalization. It is clear that normalization reduces the energy correlation.

### 3.2.1 Learning the parameters of the model

In this work, our main purpose is to observe the effects of normalization in the responses obtained at the outputs of a convolutional layer in a deep CNN. For this reason, we apply the flexible normalization model to the responses of filters from a pre-trained network that did not include flexible normalization<sup>3</sup>. The responses of a layer from these pre-trained network are used to construct the set of center and surround units to be normalized. The parameters of the flexible normalization model, the prior  $\Pi_{cs}$  and covariances  $\Lambda_{cs}$ ,  $\Lambda_c$ , and  $\Lambda_s$ , are then learned by EM fitting to the pre-trained CNN responses [12].

## 4 Simulations

We integrate flexible normalization into the AlexNet architecture [25] pre-trained on the ImageNet ILSVRC2012 object recognition challenge. Since our main goal is to investigate what the effects of normalization are at the layer level rather than at the network level, we only learn the parameters of the divisive normalization model on top of the pre-trained filters. The divisive normalization is applied to the outputs of the convolutional layer. In particular, we integrate flexible normalization into the outputs of the second convolutional layer of AlexNet. In our model, the center neighborhoods are the same built-in neighborhoods that were induced by the local response normalization operation carried out in the original AlexNet architecture. The surround groups are obtained by taking activations from an approximately circular neighborhood with a radius of 4, at every 45 degrees, which yields a total of 8 surround units. Figure 2a depicts the spatial arrangement of a center response and the positions of its surround responses.

### 4.1 Redundancy in activations of mid-layers

As argued above, multiplicative couplings between linear decomposition coefficients are common in natural images. These couplings can be measured by correlation of energies. We first ask how the outputs at the convolutional layer of AlexNet handles these dependencies, i.e., are filter activations statistically dependent? We examine the structure of spatial dependencies within a unit. Let  $I(x, y, k)^l$  denote the output of the  $k$  convolutional unit from layer  $l$  at spatial location  $x, y$ . We show that even at spatial locations for which the filters have less than 20% overlap, the values of the activations of spatially shifted units are correlated beyond first order<sup>4</sup>. In Figure 2b, we display the energy correlations for the activations of a subset of units in the second convolutional layer (Conv2) of AlexNet. For each unit, we display the correlation of energies between the given unit and its spatial neighbors 4 strides apart in either the vertical or horizontal direction. Each one of the  $3 \times 3$  tiles, is the corresponding squared correlation for a particular unit. It is possible to see that not only these high order couplings remain for the outputs of the Conv2 layer, but also the regularities in how their values are distributed in space. For various units, it is clear that spatial shifts in particular directions have stronger couplings.

<sup>3</sup>In our work, filters were trained for object recognition

<sup>4</sup>Correlations beyond first order include correlation of squares as a special case



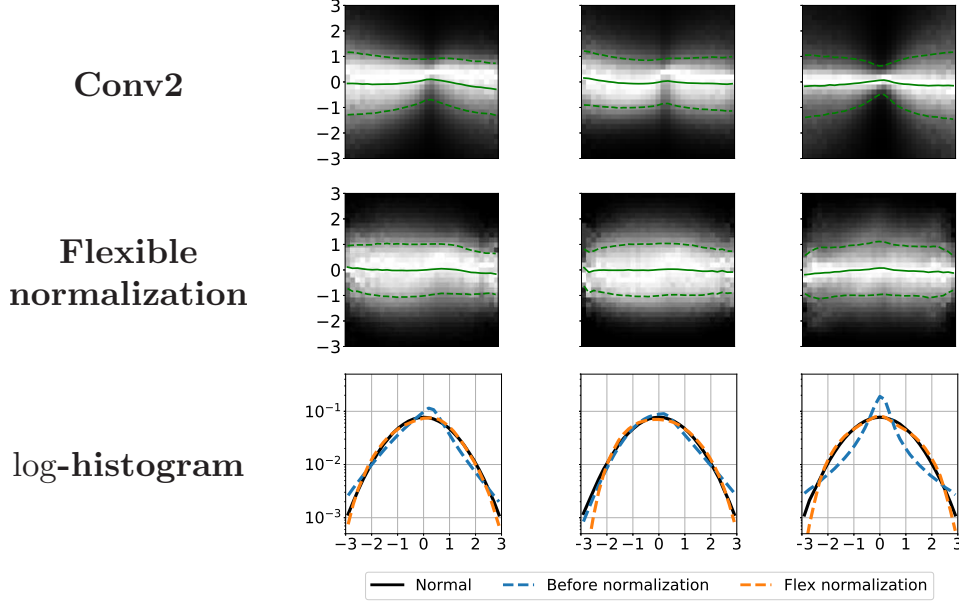


Figure 3: Marginal and normalized conditional distributions of activations from exemplar units in AlexNet. The joint conditional distributions are a simple way to visually inspect dependencies. As we can see, Conv2 units at different spatial locations are nonlinearly coupled. Flexible normalization reduces these dependencies, making the conditional distributions look closer to constant. In addition, the marginal *log*-histograms show that the normalized responses become closer to Gaussian, in agreement with the model assumptions.

#### 4.2 Dependency reduction by flexible normalization

To visually assess the effect of normalization on the correlation structure among units, we depict the joint conditional histograms of the unit activations, after normalization and whitening. Previous studies with V1-like filters have shown that filter activations follow a bowtie-like structure that can be understood as a high order coupling [36]. In particular, the amplitude of one variable gives information about the variance (standard deviation) of the other variable. This dependency can be reduced via divisive normalization from neighboring filter activations. Figure 3 shows the conditional histograms ( $p(x_s|x_c)$ ) for the same pair of center-surround unit activations before and after applying flexible divisive normalization. Along with the normalized conditional histograms, we show marginal *log*-histograms which give an idea of how normalization changes the marginal distributions from highly kurtotic to more Gaussian-like.

#### 4.3 Predicting homogeneity of stimuli based mid-level features

The main idea of flexible normalization is that contextual modulation of neural responses should be present only when responses are deemed as statistically dependent. In the case of V1, co-linearity of stimuli in the preferred direction of the center unit would cause the flexible normalization model to invoke suppression. In other words, the model would infer high center-surround posterior probability from the stimuli. In the case of mid-level features, we wanted to observe which types of stimuli would provide a similar outcome. Note that for mid-level features, the notion of orientation is not as clear as in V1, where models may contain orientations in their filter parameterizations.

Figure 4a shows some examples of image patches that cover the center-surround neighborhoods, for which the model finds a high posterior probability of Center-Surround dependence. Along with these images, a visualization of the receptive field of the second convolutional layer units is presented.

As can be seen, for some of the Conv2 representations, the idea of co-linearity is present in the form of tiling of these mid-level features. The center surround covariance also captures this property. By looking at the receptive fields of the Conv2 units (second column from the left in Figure 4a) we can see that spatial arrangements of repetitions of these receptive fields seem more natural in

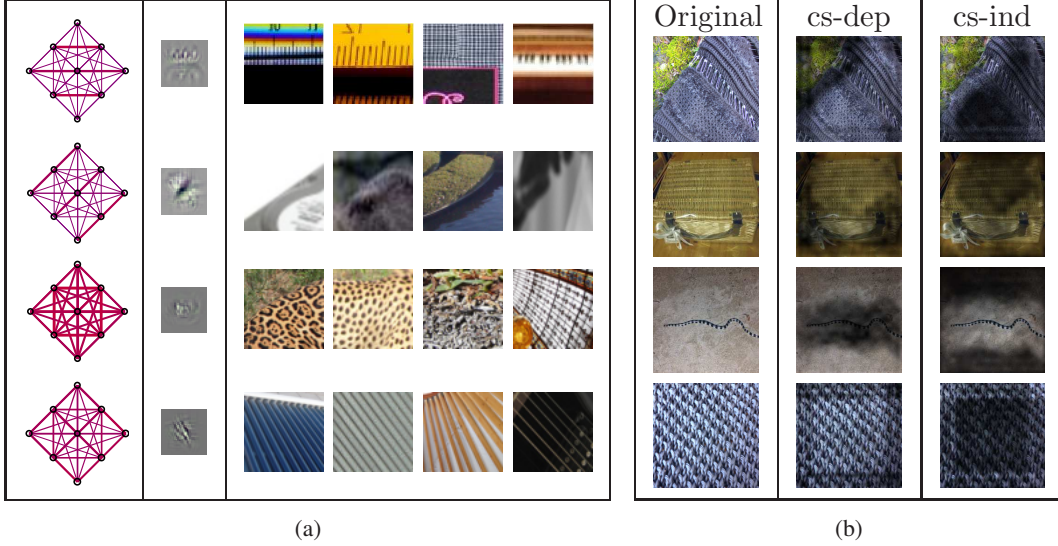


Figure 4: (a) Tiling in Conv2 center-surround dependent units. (left) center-surround dependent covariances. Each point corresponds to the spatial location of the receptive fields. Thickness of lines between points depict the strength of covariance between spatially shifted receptive fields. (middle) Conv2 units. (right) Image regions with high probability of being Center-Surround dependent according to our model. Note how regions can be seen as tiling the space with translations of the Conv2 unit receptive fields in directions with strong covariance. (b) Inferred posterior distributions on ImageNet data. (left) Original images input to the CNN. For each image at each spatial location, we compute the geometric mean of posterior probabilities among all channels of the layer (Conv2). (middle) Areas that the model deemed as dependent while obscuring other areas. (right) Complementary display where high center-surround dependent areas are darker, instead.

certain configurations. For instance, on the first row horizontal arrangements of translated versions of the receptive field give a continued pattern as appreciated in the corresponding patches (right columns). We also looked at the spatial distribution of the posterior probabilities for entire images from ImageNet. For each channel in the convolutional layer, we obtained the posterior probabilities and compute the geometric mean across channels. Figure 4b show the relation between the image content and the posterior probability by shading areas with high (middle column) and low (right column) posterior probability of being center-surround dependent. As mentioned earlier, a high posterior probability of center-surround dependent activations can be an indicator of the homogeneity of the region under consideration. As we can see, the posterior probabilities from Conv2 units capture this homogeneity at a more structured level compared to previous work on V1-like filters, where homogeneous regions correspond to elongated lines in the preferred orientations of the filters.

## 5 Discussion

In modeling normalization of V1 units, it has been observed that the learned covariance matrix (influencing the contextual normalization) has collinear structure [13]. This reflects the oriented front end of V1 units and the collinear structure prevalent in images. Our work, builds on a modified version of the model of [13] and the use of mid-level representations that are learned by convolutional networks trained for object recognition. The second convolutional layer of AlexNet combines responses from different units from the first layer into more elaborate features. However, it is not intuitively clear what is the covariance structure between such second layer units. We found in our simulations, that the learned covariances for Conv2 units do include more involved spatial arrangements, as well as collinearity. Images that were deemed as highly dependent along with the visualization of the receptive fields of the second layer units showed that the covariance structure can be attributed to tiling in more complex structures such as the boundary between two different textures (see first row of Figure 4a). Furthermore, we found that adding independence among surround units in the center-surround independent component of the mixture (25) is crucial for learning the parameters



of the model without imposing symmetry constraints. This is particularly necessary in the context of deep CNNs, and even more so at middle levels. Unlike Gabor filters or steerable pyramids, units of deep CNNs are not parametrized explicitly with respect to orientations, for instance. The same issue arises in cortical neurons, whereby higher neural areas beyond V1 combine orientations in a nonlinear manner, leading to rich structure that is not easily parameterized. The model does a good job at reducing multiplicative dependencies, but it is not perfect. Currently, filters of the CNN are not learned jointly with flexible normalization. However, the model does make predictions about when normalization might be relevant in cortical neurons to reduce redundancy in non-trivial ways. The inferred posterior probabilities expose spatial structure that matches well with some forms of homogeneity such as those present in textures. We expect our model can make useful predictions for testing normalization of neural responses to large stimuli that extend beyond the classical receptive field in higher areas of cortex.

## References

- [1] D. Andrews and C. Mallows. Scale mixtures of normal distributions. *J. Royal Stat. Soc.*, 36:99–102, 1974.
- [2] Fred Attneave. Some informational aspects of visual perception. *Psychological Review*, 61(3):183–193, 1954.
- [3] Lei Jimmy Ba, Ryan Kiros, and Geoffrey E. Hinton. Layer normalization. *CoRR*, abs/1607.06450, 2016.
- [4] Johannes Balle, Valero Laparra, and Eero P. Simoncelli. Density modelling of images using a generalized normalization transformation. In *International Conference on Learning Representations*, 2016.
- [5] Horace B. Barlow. *Possible Principles Underlying the Transformations of Sensory Messages*, chapter 13, pages 217–234. MIT press, 1961.
- [6] Anthony J. Bell and Terrence J. Sejnowski. The "independent components" of natural scenes are edge filters. *Vision Research*, 37(23):3327–3338, December 1997.
- [7] Matteo Carandini and David J. Heeger. Normalization as a canonical neural computation. *Nature Reviews, Neuroscience*, 13:51–62, January 2012.
- [8] Matteo Carandini, David J. Heeger, and J. Anthony Movshon. Linearity and normalization in simple cells of the macaque primary visual cortex. *The Journal of Neuroscience*, 17(21):8621–8644, 1997.
- [9] J. R. Cavanaugh, W. Bair, and J. A. Movshon. Nature and interaction of signals from the receptive field center and surround in macaque v1 neurons. *Journal of Neurophysiology*, 88(5):2530–2546, November 2002.
- [10] J. R. Cavanaugh, W. Bair, and J. A. Movshon. Selectivity and spatial distribution of signals from the receptive field surround in macaque v1 neurons. *Journal of Neurophysiology*, 88(5):2547–2556, November 2002.
- [11] Adam Coates and Andrew Y. Ng. Selecting receptive fields in deep networks. In J. Shawe-Taylor, R. S. Zemel, P. L. Bartlett, F. Pereira, and K. Q. Weinberger, editors, *Advances in Neural Information Processing Systems 24*, pages 2528–2536, 2011.
- [12] R. Coen-Cagli, P. Dayan, and O. Schwartz. Statistical models of linear and nonlinear contextual interactions in early visual processing. In *Advances in Neural Information Processing Systems 22*, 2009.
- [13] R. Coen-Cagli, P. Dayan, and O. Schwartz. Cortical surround interactions and perceptual salience via natural scene statistics. *PLoS Computational Biology*, 8(3), 2012.
- [14] R. Coen-Cagli, A. Kohn, and O. Schwartz. Flexible gating of contextual modulation during natural vision. *Nature Neuroscience*, 18:1648–1655, 2015.
- [15] David J. Field. Relations between the statistics of natural images and the response properties of cortical cells. *Journal of the Optical Society of America*, 4(12):2379–2394, December 1987.
- [16] Wilson S. Geisler. Visual perception and the statistical properties of natural scenes. *Annual Review of Psychology*, 59:167–192, January 2008.

- [17] J. R. Golden, K. P. Vilankar, M. C. Wu, and D. J. Field. Conjectures regarding the nonlinear geometry of visual neurons. *Vision Research*, 120:74–92, March 2016.
- [18] Sunhyoung Han and Nuno Vasconcelos. Biologically plausible saliency mechanisms improve feedforward object recognition. *Vision research*, 50(22):2295–2307, 2010.
- [19] Sunhyoung Han and Nuno Vasconcelos. Object recognition with hierarchical discriminant saliency networks. *Frontiers in computational neuroscience*, 8, 2014.
- [20] David J. Heeger. Normalization of cell responses in cat striate cortex. *Visual Neuroscience*, 9:181–197, 1992.
- [21] Aapo Hyvärinen, Jarmo Hurri, , and Patrik O. Hoyer. *Natural Image Statistics: A probabilistic approach to early computational vision*. Springer, 2009.
- [22] Sergey Ioffe and Christian Szegedy. Batch normalization: Accelerating deep network training by reducing internal covariate shift. In *Proceedings of the 32Nd International Conference on International Conference on Machine Learning - Volume 37*, ICML’15, pages 448–456. JMLR.org, 2015.
- [23] Kevin Jarrett, Koray Kavukcuoglu, Marc’ Aurelio Ranzato, and Yann LeCun. What is the best multi-stage architecture for object recognition? In *ICCV*, pages 2146–2153. IEEE, 2009.
- [24] Yan Karklin and Michael S. Lewicki. Emergence of complex cell properties by learning to generalize in natural scenes. *Nature*, 457(1):83–87, January 2009.
- [25] A. Krizhevsky, I. Sutskever, and G. E. Hinton. Imagenet classification with deep convolutional neural networks. In *Neural Information Processing Systems*, 2012.
- [26] Jonathan B. Levitt and Jennifer S. Lund. Contrast dependence of contextual effects in primate visual cortex. *Nature*, 387:73–76, May 1997.
- [27] Z. Li. Visual segmentation by contextual influences via intra-cortical interactions in the primary visual cortex. *Network*, 10(2):187–212, May 1999.
- [28] Timm Lochmann, Udo A. Ernst, and Sophie Deneve. Perceptual inference predicts contextxxual modulations of sensory responses. *Journal of Neuroscience*, 32(12):4179–4195, March 2012.
- [29] Bruno A. Olshausen and David J.Field. Sparse coding with an overcomplete basis set: A strategy employed by v1? *Vision Research*, 37(23):3311–3325, 1997.
- [30] Bruno A. Olshausen and Michael S. Lewicki. What natural scenes statistics can tell us about cortical representation. *The New Visual Neurosciences*, pages 1247–1262, 2014.
- [31] Tomaso Poggio and Fabio Anselmi. *Visual Cortex and Deep Networks: Learning Invariant Representations*. MIT Press, 2016.
- [32] Rajesh P.N. Rao and Dana H. Ballard. Predictive coding in the visual cortex: a fuctional interpretation of some extra-classical receptive-field effects. *Nature Neuroscience*, 2(1):79–87, January 1999.
- [33] Mengye Ren, Renjie Liao, Raquel Urtasun, Fabian H. Sinz, and Richar S. Zemel. Normalizing the normalizers: Comparing and extending network normalization schemes. In *Proceedings of the 5th International Conference on Learning Representations*, ICLR 2017, 2017.
- [34] Michael P. Sceniak, Dario L. Ringach, Michael J. Hawken, and Robert Shapley. Contrast’s effect on spatial summation by macaque v1 neurons. *Nature Neuroscience*, 2(8):733–739, August 1999.
- [35] O. Schwartz, T.J. Sejnowski, and P. Dayan. Perceptual organization in the tilt illusion. *Journal of Vision*, 9(4)(19):1–20, 2009.
- [36] Odelia Schwartz and Eero P. Simoncelli. Natural signal statistics and sensory gain control. *Nature Neuroscience*, 4(8):819–825, August 2001.
- [37] Eero P. Simoncelli. Statistical models for images: Compression, restoration and synthesis. In *31st Asilomar Conference on Signals, Systems, and Computers*, pages 673–678. IEEE Computer Society, November 1997.
- [38] Eero P. Simoncelli and Bruno A. Olshausen. Natural image statistics nad neural representation. *Annual Reviews Neuroscience*, 24:1193–1216, 2001.

- [39] Karen Simonyan and Andrew Zisserman. Very deep convolutional networks for large-scale image recognition. In *Proceedings of the 3rd International Conference on Learning Representations*, ICLR 2015, 2015.
- [40] M. W. Spratling. Predictive coding as a model of response properties in cortical area v1. *Journal of Neuroscience*, 30(9):3531–3543, March 2010.
- [41] M J Wainwright and E P Simoncelli. Scale mixtures of Gaussians and the statistics of natural images. In S. A. Solla, T. K. Leen, and K.-R. Müller, editors, *Adv. Neural Information Processing Systems*, volume 12, pages 855–861, Cambridge, MA, May 2000. MIT Press.
- [42] M. J. Wainwright, E. P. Simoncelli, and A. S. Willsky. Random cascades on wavelet trees and their use in modeling and analyzing natural imagery. *Applied and Computational Harmonic Analysis*, 11(1):89–123, July 2001. Special issue on wavelet applications.
- [43] Bernhard Wegmann and Christoph Zetsche. Visual-system-based polar quantization of local amplitude and local phase of orientation filter outputs. In *Human Vision and Electronic Imaging: Models, Methods, and Applications*, volume 1249, 1990.
- [44] Daniel L.K. Yamins and James J DiCarlo. Using goal-driven deep learning models to understand sensory cortex. *Nature Neuroscience*, 19(3):356–365, March 2016.
- [45] C. Zetsche and U. Nuding. Nonlinear and higher-order approaches to the encoding of natural scenes. *Network*, 16(2-3):191–221, June–September 2005.
- [46] L. Zhaoping. Theoretical understanding of the early visual processes by data compression and data selection. *Network*, 17(4):301–334, December 2006.
- [47] Mengchen Zhu and Christopher J. Rozell. Visual nonclassical receptive field effects emerge from sparse coding in a dynamical system. *PLOS Computational Biology*, 9(8), August 2013.
- [48] Corey M. Ziemba, Jeremy Freeman, Eero P. Simoncelli, and J. Anthony Movshon. Contextual modulation of sensitivity to naturalistic image structure in macaque v2. *Journal of Neurophysiology*, 2018.

## A Technical details

### A.1 Maximum likelihood estimation of covariance

Recall the pdf of our Gaussian scale mixture with Rayleigh mixer:

$$p_X(\mathbf{x}) = \frac{1}{(2\pi)^{m/2} |\mathbf{\Lambda}|^{1/2} h^m} a^{1-m/2} K_{m/2-1}(a), \quad (10)$$

where  $K_\lambda(\cdot)$  is the modified Bessel function of the second kind, and

$$a^2 = \frac{\mathbf{x}^T \mathbf{\Lambda}^{-1} \mathbf{x}}{h^2}. \quad (11)$$

Equation (10) can be employed to compute the likelihood function of the covariance matrix  $\mathbf{\Lambda}$ . Furthermore, notice that the scale parameter  $h$  can be simply dismissed by making part of the covariance<sup>5</sup>. If we take  $\hat{\mathbf{\Lambda}}^2 = \mathbf{\Lambda} h^2$ , (10) becomes:

$$p_X(\mathbf{x}) = \frac{1}{(2\pi)^{m/2} |\hat{\mathbf{\Lambda}}|^{1/2}} \hat{a}^{1-m/2} K_{m/2-1}(\hat{a}), \quad (12)$$

where  $\hat{a} = \mathbf{x}^T \hat{\mathbf{\Lambda}}^{-1} \mathbf{x}$ . From this point on, to simplify notation, we will refer to  $\hat{\mathbf{\Lambda}}$  as  $\mathbf{\Lambda}$ . and  $\hat{a}$  as simply  $a$ .

For an exemplar  $\mathbf{x}_i$ , the partial derivative of log-likelihood function with respect to  $\mathbf{\Lambda}^{-1}$  is given by:

$$\begin{aligned} \frac{\partial \log L(\mathbf{\Lambda}|\mathbf{x}_i)}{\partial \mathbf{\Lambda}^{-1}} &= \frac{\partial \log(p_X(\mathbf{x}_i))}{\partial \mathbf{\Lambda}^{-1}} = \frac{1}{p_X(\mathbf{x}_i)} \frac{\partial p_X(\mathbf{x}_i)}{\partial \mathbf{\Lambda}^{-1}} \\ &= \frac{\mathbf{\Lambda}}{2} - \frac{1}{2a} \frac{K_{m/2}(a)}{K_{m/2-1}(a)} \mathbf{x}_i \mathbf{x}_i^T. \end{aligned} \quad (13)$$

---

<sup>5</sup>Adding scale back is straightforward.

Based on (13), we propose the following iterative update rule for  $\Lambda$

$$\Lambda_{\text{new}} \leftarrow \frac{1}{N} \sum_{i=1}^N g_m(a_i) \mathbf{x}_i \mathbf{x}_i^T, \quad (14)$$

where

$$g_m(a_i) = \frac{1}{a_i} \frac{K_{m/2}(a_i)}{K_{m/2-1}(a_i)}, \quad (15)$$

and  $a_i = \sqrt{\mathbf{x}_i^T \Lambda_{\text{old}}^{-1} \mathbf{x}_i}$ .

### A.1.1 Details about inference

Here, we work out the inference procedure for the full covariance GSM. Let  $\setminus i$  denote the set of all indexes minus index  $i$ , and decompose the precision matrix  $\Lambda^{-1}$  into,

$$\Lambda^{-1} = \begin{bmatrix} (\Lambda^{-1})_{\setminus i, \setminus i} & (\Lambda^{-1})_{\setminus i, i} \\ (\Lambda^{-1})_{i, \setminus i} & (\Lambda^{-1})_{i, i} \end{bmatrix}. \quad (16)$$

It can be shown that

$$\mathbb{E}[G_i | \mathbf{x}] = \frac{c_i}{\sqrt{a_{\setminus i}}} \left( \frac{a}{a_{\setminus i}} \right)^{\frac{m}{2}-1} \frac{|\Lambda|^{\frac{1}{2}}}{\sigma_i |((\Lambda^{-1})_{\setminus i, \setminus i})^{-1}|^{\frac{1}{2}}} \frac{K_{\frac{m-1}{2}}(a_{\setminus i})}{K_{\frac{m}{2}-1}(a)}, \quad (17)$$

where  $\sigma_i^2 = (\Lambda)_{i, i}$ , and

$$\begin{aligned} a_{\setminus i}^2 &= \mathbf{x}_{\setminus i}^T (\Lambda^{-1})_{\setminus i, \setminus i} \mathbf{x}_{\setminus i} + 2x_i \mathbf{x}_{\setminus i}^T (\Lambda^{-1})_{\setminus i, i} + \\ &+ x_i^2 [(\Lambda^{-1})_{i, \setminus i} ((\Lambda^{-1})_{\setminus i, \setminus i})^{-1} (\Lambda^{-1})_{\setminus i, i} + \sigma_i^{-2}]. \end{aligned} \quad (18)$$

Noticing that

$$(\Lambda^{-1})_{i, i} = \sigma_i^{-2} + (\Lambda^{-1})_{i, \setminus i} ((\Lambda^{-1})_{\setminus i, \setminus i})^{-1} (\Lambda^{-1})_{\setminus i, i}, \quad (19)$$

yields  $a_{\setminus i} = a$ . Furthermore, since  $\sigma_i^2 = |\Lambda| |(\Lambda^{-1})_{\setminus i, \setminus i}|$ ,

$$\mathbb{E}[G_i | \mathbf{x}] = \frac{x_i}{\sqrt{a}} \frac{K_{\frac{m-1}{2}}(a)}{K_{\frac{m}{2}-1}(a)}. \quad (20)$$

## B Mixture of Gaussian Scale Mixtures

The mixture model has the following general form:

$$p_X(\mathbf{x}) = \sum_{\alpha \in \mathcal{A}} \Pi_{\alpha} p_X(\mathbf{x} | \Lambda_{\alpha}) \quad (21)$$

Parameter estimation for the above model (21) can be solved using expectation maximization (EM) algorithm. In particular, we use the conditional EM algorithm to update the parameters of each of the mixture components. For each partial **E-step**, we compute the posterior distributions over the assignment variable:

$$q(\alpha, \mathbf{x}_i) = \frac{\Pi_{\alpha} p_X(\mathbf{x}_i | \Lambda_{\alpha})}{\sum_{\alpha' \in \mathcal{A}} \Pi_{\alpha'} p_X(\mathbf{x}_i | \Lambda_{\alpha'})}, \text{ for all } \alpha \in \mathcal{A}. \quad (22)$$

In the partial **M-step**, we update all the mixture probabilities using (22),

$$\Pi_{\alpha'} \leftarrow \frac{1}{N} \sum_{i=1}^N q(\alpha', \mathbf{x}_i), \text{ for all } \alpha' \in \mathcal{A}, \quad (23)$$

and the corresponding covariance  $\Lambda_{\alpha}$  using a modified version of the fixed-point (14), as follows:

$$\Lambda_{\alpha} \leftarrow \frac{\sum_{i=1}^N q(\alpha, \mathbf{x}_i) g_m(\mathbf{x}_i | \Lambda_{\alpha}) \mathbf{x}_i \mathbf{x}_i^T}{\sum_{j=1}^N q(\alpha, \mathbf{x}_j)}. \quad (24)$$

where  $g_m(\mathbf{x}_i | \Lambda_{\alpha}) = g_m(\sqrt{\mathbf{x}_i^T \Lambda_{\alpha}^{-1} \mathbf{x}_i})$  from (15). We use a single fixed-point iteration per partial CEM iteration. The proposed fixed point update increases the likelihood at each iteration.

### B.1 Two-GSM mixture model for Flexible Normalization

Gaussian scale mixture models have been used to explain non-linear dependencies among linear decompositions of natural stimuli such as images. In the simplest case, it is assumed that such dependencies carry over the entire stimuli. For example, in vision, commonly used approaches of local contrast normalization apply the same normalization scheme across the entire image. Spatial pools for normalization have been applied to explain responses to redundant stimuli. While this model is able to account for suppressions of unit responses where spatial context is redundant, it can also lead to suppression in cases where context may not be redundant. A flexible normalization that suppresses responses only when the spatial context is deemed as redundant can be constructed as a mixture of GSMs. A simple version considers a component with full center-surround dependencies, a second component representing the center-surround independence results from the product of a center only and surround only GSM distributions:

$$p_X(\mathbf{x}) = \Pi_{cs} p_X(\mathbf{x}|\mathbf{\Lambda}_{cs}) + (1 - \Pi_{cs}) p_{X_c}(\mathbf{x}_c|\mathbf{\Lambda}_c) p_{X_s}(\mathbf{x}_s|\mathbf{\Lambda}_s), \quad (25)$$

where  $\mathbf{x}_c$  and  $\mathbf{x}_s$  denote the sub-vectors of  $\mathbf{x}$  containing the center and surround variables, respectively. The variants of the EM steps presented in (22), (23), and (24) are discussed below. For each partial **E-step**

$$q(cs, \mathbf{x}_i) = \frac{\Pi_{cs} p_X(\mathbf{x}_i|\mathbf{\Lambda}_{cs})}{Q(\mathbf{x}_i)}, \quad (26)$$

$$q(cs \perp, \mathbf{x}_i) = \frac{(1 - \Pi_{cs}) p_{X_c}(\mathbf{x}_{i,c}|\mathbf{\Lambda}_c) p_{X_s}(\mathbf{x}_{i,s}|\mathbf{\Lambda}_s)}{Q(\mathbf{x}_i)} = 1 - q(cs, \mathbf{x}_i) \quad (27)$$

$$Q(\mathbf{x}_i) = \Pi_{cs} p_X(\mathbf{x}_i|\mathbf{\Lambda}_{cs}) + (1 - \Pi_{cs}) p_{X_c}(\mathbf{x}_{i,c}|\mathbf{\Lambda}_c) p_{X_s}(\mathbf{x}_{i,s}|\mathbf{\Lambda}_s) \quad (28)$$

$$(29)$$

Each partial **M-step** updates the center-surround dependent probability using (22),

$$\Pi_{cs} \leftarrow \frac{1}{N} \sum_{i=1}^N q(cs, \mathbf{x}_i). \quad (30)$$

Three partial **M-step** updates are required:

1. A center-surround dependent covariance  $\mathbf{\Lambda}_{cs}$  update,

$$\mathbf{\Lambda}_c \leftarrow \frac{\sum_{i=1}^N q(cs, \mathbf{x}_i) g_m(\mathbf{x}_i|\mathbf{\Lambda}_{cs}) \mathbf{x}_i \mathbf{x}_i^T}{\sum_{j=1}^N q(cs, \mathbf{x}_j)}, \quad (31)$$

2. a center-only covariance

$$\mathbf{\Lambda}_c \leftarrow \frac{\sum_{i=1}^N (1 - q(cs, \mathbf{x}_i)) g_{m_c}(\mathbf{x}_{i,c}|\mathbf{\Lambda}_c) \mathbf{x}_{i,c} \mathbf{x}_{i,c}^T}{\sum_{j=1}^N 1 - q(cs, \mathbf{x}_j)}. \quad (32)$$

3. and a surround-only covariance

$$\mathbf{\Lambda}_s \leftarrow \frac{\sum_{i=1}^N (1 - q(cs, \mathbf{x}_i)) g_{m_s}(\mathbf{x}_{i,s}|\mathbf{\Lambda}_s) \mathbf{x}_{i,s} \mathbf{x}_{i,s}^T}{\sum_{j=1}^N 1 - q(cs, \mathbf{x}_j)}. \quad (33)$$

#### Re-parameterization:

To simplify computations and directly enforce the nonnegative definiteness in our covariance estimation, we re-parametrize the likelihood function. Let us write,

$$\mathbf{\Lambda} = \mathbf{B}^T \mathbf{B}, \text{ and } \mathbf{\Lambda}^{-1} = \mathbf{A}^T \mathbf{A}. \quad (34)$$



Then,  $\mathbf{B} = \mathbf{A}^{-\text{T}}$  and

$$\frac{\partial \log L(\mathbf{A}|\mathbf{x}_i)}{\partial \mathbf{A}} = \mathbf{B} - \frac{1}{a} \frac{K_{m/2}(a)}{K_{m/2-1}(a)} \mathbf{A} \mathbf{x}_i \mathbf{x}_i^{\text{T}}, \quad (35)$$

which yields the following fixed point update:

$$\mathbf{B}_{\text{new}} \leftarrow \frac{1}{N} \sum_{i=1}^N g_m(a_i) \mathbf{A}_{\text{old}} \mathbf{x}_i \mathbf{x}_i^{\text{T}} \quad (36)$$

### B.1.1 A center-surround independent model with independent surround units

In this model the center surround independent component has the extra property that requires surround units to be independent from each other. One consequence of this requirement is that the surround covariance  $\mathbf{\Lambda}_s$  becomes a diagonal matrix. Note that diagonal covariance is a necessary but not sufficient condition for independence in this case. The main feature for independence is that each one of the surround units has its own mixer (scaling rather than mixing) variable instead of a shared mixer as it is the case in the model previously discussed. If the mixer (scaling) variables are Rayleigh distributed, each surround unit  $\ell$  in the center-surround independent component has a Laplace distribution:

$$f_{\ell}(x) = \frac{1}{2\sqrt{(\mathbf{\Lambda}_c)_{\ell,\ell}}} \exp\left(-\frac{|x|}{\sqrt{(\mathbf{\Lambda}_c)_{\ell,\ell}}}\right), \quad (37)$$

where  $(\mathbf{\Lambda}_c)_{\ell,\ell}$  denotes the diagonal element of the surround covariance matrix  $\mathbf{\Lambda}_c$ . Note that this matrix has zero off-diagonal elements by definition. In this model,

$$p_{X_s}(\mathbf{x}_{i,s}|\mathbf{\Lambda}_s) = \prod_{\ell \in S} f_{\ell}((\mathbf{x}_{i,s})_{\ell}) \quad (38)$$

In this modified version (33) becomes:

$$(\mathbf{\Lambda}_s)_{\ell,\ell} \leftarrow \frac{\sum_{i=1}^N (1 - q(\text{cs}, \mathbf{x}_i)) |(\mathbf{x}_{i,s})_{\ell}|}{\sum_{j=1}^N 1 - q(\text{cs}, \mathbf{x}_j)} \sqrt{(\mathbf{\Lambda}_s)_{\ell,\ell}}. \quad (39)$$

The rest of the **EM** algorithm proceeds in the same way as described in (31) and (32).

### B.1.2 Matching Covariances for Inference

Here, we describe how we obtain the transformation  $\mathbf{Q}$  for equation (7) in the paper. Assuming that both matrices are full rank, we can write  $\mathbf{\Lambda}_{\text{cs}} = \mathbf{A}^{\text{T}} \mathbf{A}$  and  $\mathbf{\Lambda}_{\text{cs}\perp} = \mathbf{B}^{\text{T}} \mathbf{B}$ . Furthermore, there exists a transformation  $\mathbf{Q}$  such that:

$$\mathbf{Q}^{\text{T}} \mathbf{\Lambda}_{\text{cs}\perp} \mathbf{Q} = \mathbf{\Lambda}_{\text{cs}}, \quad (40)$$

which is simply given by  $\mathbf{Q} = \mathbf{B}^{-1} \mathbf{A}$ .

## B.2 Judging the effectiveness of normalization

As noted above, the Gaussian scale mixture introduces a multiplicative coupling between variables that cannot be removed by linear means. This coupling is captured by a simple dependency measure based on the energy of the variables. For zero mean, unit variance, and mutually independent  $G_i$  and  $G_j$ , define  $X_i = C_i V$  and  $X_j = G_j V$  where mixer  $V$  is also independent of  $G_i$  and  $G_j$ . The covariance of  $X_i^2$  and  $X_j^2$  is given by

$$\begin{aligned} \mathbb{E}[(X_i^2 - \mathbb{E}[X_i^2])(X_j^2 - \mathbb{E}[X_j^2])] &= \mathbb{E}[X_i^2 X_j^2] - \mathbb{E}[X_i^2] \mathbb{E}[X_j^2] \\ &= \mathbb{E}[G_i^2 V^2 G_j^2 V^2] - \mathbb{E}[G_i^2 V^2] \mathbb{E}[G_j^2 V^2] \\ &= \mathbb{E}[V^4] - \mathbb{E}[V^2]^2. \end{aligned} \quad (41)$$

The strength of the coupling depends on the spread of  $V$ . A perfect inversion of the coupling, which would require explicit values of  $V$ , would make the expression (41) zero. Here, we use a related

measure, the correlation between squared responses [11]. This measure has been used to select groups of receptive fields that should be processed together in a subsequent layer of a deep network. The correlation between squared responses is computed in a two-step process. First, variables  $X$  are decorrelated by whitening using ZCA. For the pair whitened variables  $(\tilde{X}_i, \tilde{X}_j)$ , correlation of squared responses is given by:

$$S(\tilde{X}_i, \tilde{X}_j) = \frac{\mathbb{E}[(\tilde{X}_i^2 \tilde{X}_j^2 - 1)]}{\sqrt{\mathbb{E}[(\tilde{X}_i^4 - 1)] \mathbb{E}[(\tilde{X}_j^4 - 1)]}} \quad (42)$$

## C Additional experiments

### C.1 Flexible Normalization on the First Convolutional Layer of AlexNet

We also trained our flexible normalization model on the responses of the first convolutional layer of AlexNet. The filters on this layer resemble the patterns that have been identified to elicit vigorous responses in V1 neurons. This is not the first time the flexible normalization model has been applied to filter modeling V1. For previous work, we refer the readers to [12, 13, 14]. Nevertheless, to the best of our knowledge this is the first time the flexible normalization model has been applied to filters learned from data in a supervised learning task. In previous work, the orientation of the filters, which was known, was employed to restrict the model fitting by adding symmetry constraints to the covariance matrices of the model. As we explained in the main text, our modified model does not employ these symmetry constraints, but forces the surround variables to be fully independent, which translates into having a separate mixer variable for each one of them.

#### C.1.1 Covariance structure of the surround components of the first convolutional AlexNet

Similarly to Figure 4a in the paper, we visualize the covariance structure of the surround covariance (Figure 5). As we can see, low frequency filters expose stronger correlation in their responses than the high frequency filters. Also the orientation of the filter is reflected on the covariance structure of the model.

#### C.1.2 High order correlations between surround components of the first convolutional layer of AlexNet

Here, we show the correlation of energies for the first layer units of AlexNet before and after normalization (Figure 6). It can be seen how the normalization procedure reduces the energy correlation significantly. In addition to the squared correlation, we also visualize the normalized conditional histograms before and after normalization, as well as the marginal distributions of the center variable.

### C.2 Single GSM Normalization of Second Layer Units of AlexNet

In addition to flexible normalization, we looked at a simpler model which assumes the coupling between center and surround units remains the same across the entire image. This model is a particular case of the flexible normalization where  $\Pi_{cs} = 1$ . In this model, only the center surround dependent covariance  $\Lambda_{cs}$  is of interest.

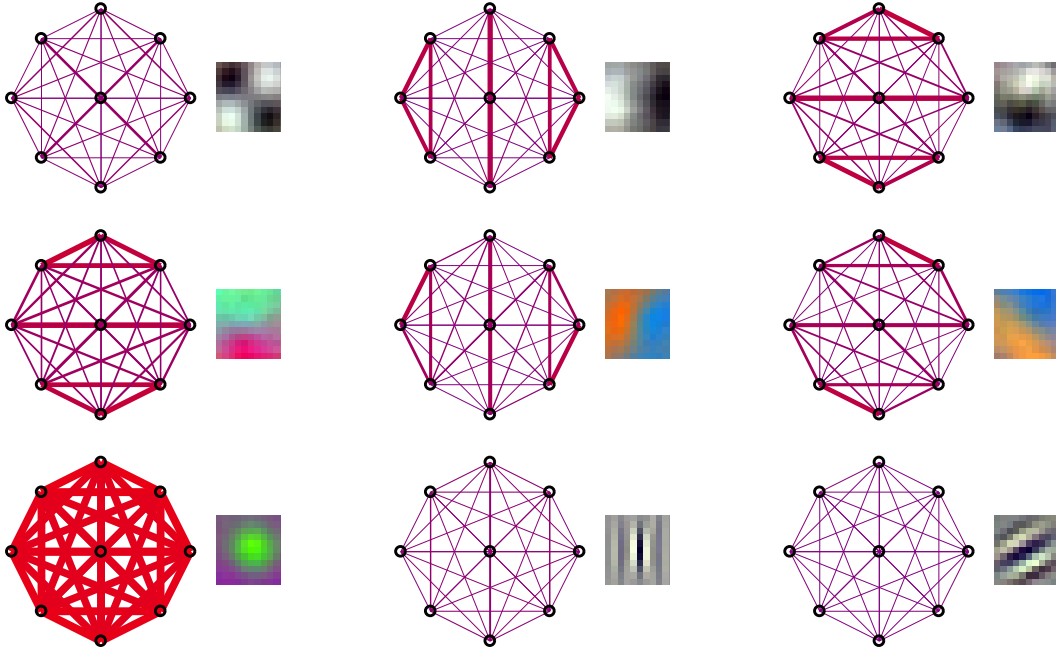


Figure 5: Covariance structure for different units in the first convolutional layer of AlexNet. We display the covariance structure of the surround pool along with the visualization of the corresponding filter. Thicker lines mean larger magnitude of the correlation. Line color linearly interpolates from blue for negative values to red for positive values

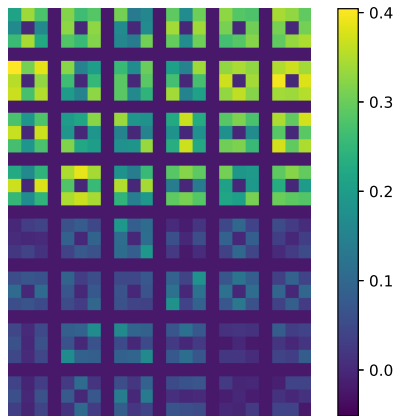


Figure 6: Correlation of energies between center and surround responses for a subset of units of the first convolutional layer of AlexNet. The upper half correspond to the correlation before normalization and the bottom half after flexible normalization.

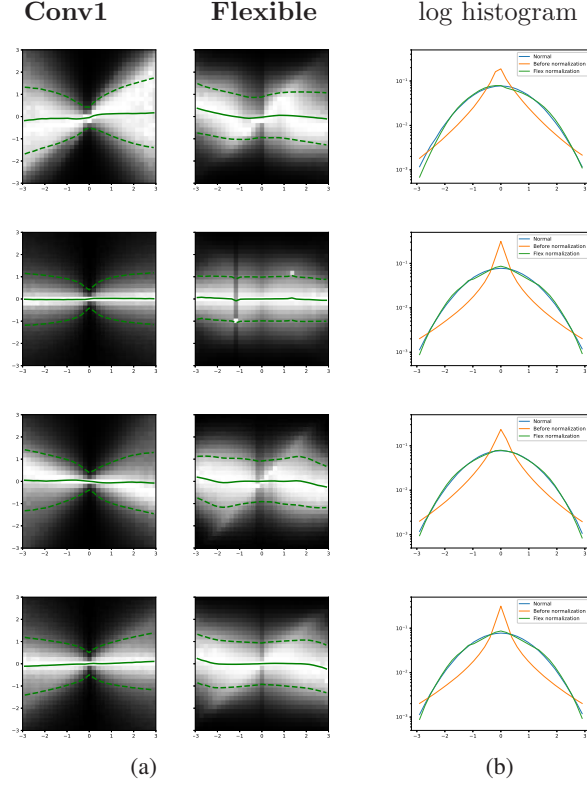


Figure 7: Normalized conditional histograms between center and surround responses from the first convolutional layer of AlexNet. Figure 7a shows the conditional distributions before and after flexible normalization. Figure 7b shows the log histograms.

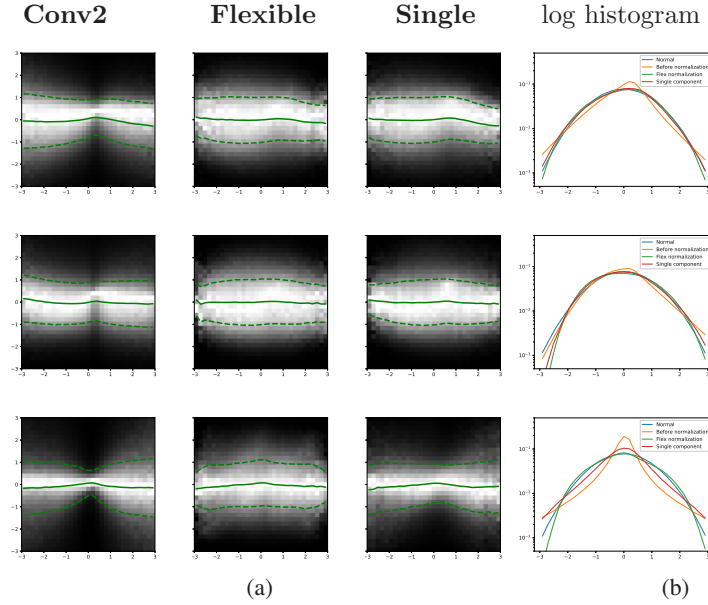


Figure 8: Comparison between flexible and single GSM normalized conditional histograms between center and surround responses from the second convolutional layer of AlexNet. Figure 8a shows the conditional distributions before and after flexible normalization and single GSM normalization. Figure 8b shows the corresponding log-histograms.